pubs.acs.org/ac Technical Note

Providing Enhanced Migration Time Reproducibility with a High-Voltage-Compatible Flow Sensor for Capillary Electrophoresis

Florian Kehl,* Tomas Drevinskas, Jessica S. Creamer, Andrew J. DeMartino, and Peter A. Willis

Cite This: https://doi.org/10.1021/acs.analchem.2c00038 Read Online

ACCESS | Metrics & More | Article Recommendations | Supporting Information

ABSTRACT: In capillary electrophoresis (CE), analyte identification is primarily based on migration time, which is a function of the analyte's electrophoretic mobility and the electro-osmotic flow (EOF). The migration time can be impacted by the presence of parasitic flow from changes in temperature or pressure during the run. Presented here is a high-voltage-compatible flow sensor capable of monitoring the volumetric flow inside the capillary during a separation with nL/min resolution. The direct measurement of both flow and time allows for compensation of flow instabilities. By expressing the electropherogram in terms of signal versus electromigration velocity instead of time, it is possible to improve the run-to-run reproducibility up to 25×.

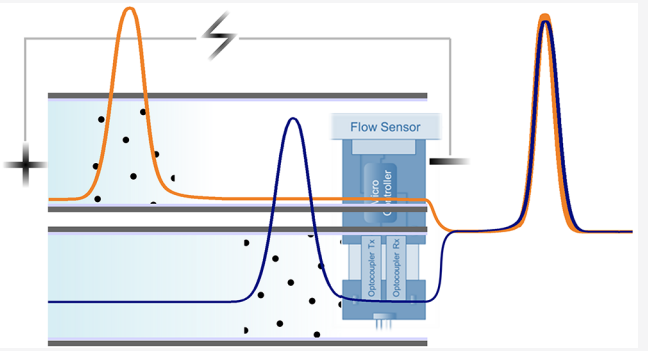

Electrophoretic separation techniques such as capillary electrophoresis (CE) provide rapid and high-efficiency separations. For this reason, novel, CE-based instruments for point-of-care, remote, *in situ*, and autonomous operation are being developed for a broad range of applications.[1−10] In portable, low fidelity systems, the voltage-driven electro-osmotic flow (EOF) can be altered by uncontrolled operating temperatures and parasitic flow induced by pressure or gravity. These effects lead to irreproducible migration times and can confound analyte identification.

To account for these changes in the migration time, it is possible to use computerized time scale compensation in CE, which mainly focuses on peak mobility recalculation based on an EOF marker, internal standard reference, thermal time marks, or a two-step method.[11−16] Unfortunately, recalculation approaches fail in cases where EOF fluctuations are unpredictable and nonlinear.[11] While thermal marks are capable of handling cases where the change of EOF velocity fluctuates, they introduce baseline distortion spikes that can interfere with the peaks of the analytes.[12]

In this publication, we describe how to continuously measure the flow and temperature inside the capillary during the separation to compensate for parasitic flow contributions and improve run-to-run reproducibly.

EXPERIMENTAL SECTION

Theoretical Model. In CE, the solutes in the sample plug migrate toward the detector once an electric potential is applied (Figure 1A). This migration velocity (ν_p) of an analyte can be expressed as

$$\nu_p = \frac{l_{\text{eff}}}{t_p} \tag{1}$$

where l_{eff} is the effective length of the capillary (in m) and t_p is the migration time of the analyte to the detector. The migration time is what is commonly plotted in an electropherogram ("peak position"). The observed migration velocity does not reflect the true electromigration velocity of the analyte but is composed of two vectors:

$$\nu_p = \nu_a + \nu_Q \tag{2}$$

where ν_a is the electromigration velocity of the analyte (in m/s) and ν_Q is the actual flow velocity of the background electrolyte (BGE) (in m/s). If the volumetric flow rate Q (in L/s) inside the capillary is measured and known, then ν_Q can be calculated with

$$\nu_Q = \frac{Q}{V_{1m}} \tag{3}$$

where V_{1m} is the volume that a 1 m length capillary channel occupies (in L). In CE, ν_Q itself has two contributors, the electro-osmotic flow velocity ν_{EOF} (driven by the EOF), and the parasitic flow velocity, ν_{PF}.

$$\nu_Q = \nu_{EOF} + \nu_{PF} \tag{4}$$

Received: January 4, 2022
Accepted: March 22, 2022

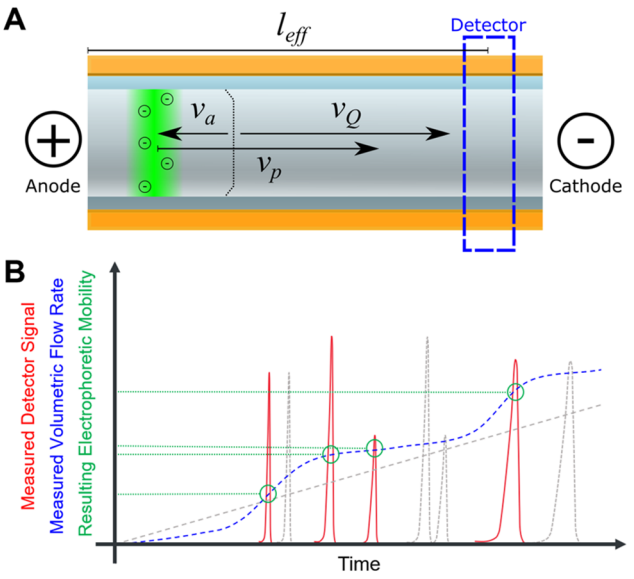

Figure 1. (A) Section view of a capillary. The sample's migration during a separation can be described with the migration velocity vectors $\boldsymbol{v}_p$, as a result of the superposition of the volumetric flow velocity $\boldsymbol{v}_Q$, and the electromigration velocity of the analyte $\boldsymbol{v}_a$ itself. (B) When flow in the capillary is constant, peak spacing on the time axis is proportional to migration time (gray). When flow varies during a separation (as is shown here by the dashed blue curve) it directly influences the migration times of the analyte peaks (red). When the flow rate is known, it is possible to compensate for this parasitic flow and calculate the electrophoretic velocity of the analytes (green).

Parasitic flow contributions include pressure- or gravity-driven flow. The analyte's migration time through the separation process is affected by the variation in flow rate that was observed before the peak was detected. Therefore, the average previous flow rate up to time t_m is calculated. This can be expressed as $\boldsymbol{v}_{Q_e}$.

$$\boldsymbol{v}_{Q_e}(i) = \frac{\sum_{i=1}^{I}(\boldsymbol{v}_{Qi} \times \Delta_{ti})}{t_p}, \quad i = 1, \ 2, \ \cdots I \tag{5}$$

where $\boldsymbol{v}_{Q_e}(i)$ is the average linear velocity of the flow rate (in m/s), i is a data point number, and I is a data point number at t_p, the recorded migration time of the peak, $\boldsymbol{v}_{Q_i}$ the flow velocity at data point i, Δ_{t_i} is the discretization period (in s) at data point i, and t_p the migration time of the analyte (in s).

With eq 5, the electromigration velocity ($\boldsymbol{v}_a$) of the analyte (m/s) can then be calculated as

$$\boldsymbol{v}_a = \boldsymbol{v}_p - \boldsymbol{v}_{Q_e} \tag{6}$$

where $\boldsymbol{v}_a$ is the observed migration velocity of the analyte that corresponds to a certain peak (in m/s) and $\boldsymbol{v}_{Q_e}(i)$ is the average linear velocity of the flow rate (in m/s). (Note here the migration velocity is expressed in cm/min instead of m/s, as centimeters and minutes are more commonly used in CE.)

Figure 1B is a visual representation of how measuring the volumetric flow and expressing the acquired data as flow compensated analyte electromigration velocity can dramatically increase the reproducibility of CE experiments.

Besides correcting for parasitic flow contributions by measuring the volumetric flow during a separation, we also introduce an optional second step to correct for Joule heating and separation voltage-induced effects. Joule heating, and hence the increase in temperature, is a result of the electrical current flowing through the capillary due to the applied electric potential.[17] Joule heating (and other effects) results in a voltage−current nonlinearity. Therefore, as a first-order approximation, Joule heating and hence the temperature can be approximated by the relative increase of the separation current. We here express the results of CE measurements in an instrument-independent manner by dividing the analyte electromigration velocity $\boldsymbol{v}_a$ by the separation current I_S, or if expressed in SI units, meters per second divided by Amperes. Since Amperes are equal to Coulombs per second, the resulting unit is meters per Coulomb.

$$\frac{\boldsymbol{v}_a}{I_s} \rightarrow \frac{(\mathrm{m/s})}{(\mathrm{A})} \rightarrow \frac{(\mathrm{m/s})}{(\mathrm{C/s})} \rightarrow \frac{(\mathrm{m})}{(\mathrm{C})} \tag{7}$$

First, it has to be noted that time and voltage have now been eliminated entirely from the equation. Second, m/C should be understood as "charge separation", or as the distance which the analyte travels in the BGE per one Coulomb spent to propel the electromigration.

This work demonstrates how this method allows for the alignment of electropherograms performed at completely different voltages, which would not be the case if the results were plotted versus time.

High Voltage Flow Sensor. High-resolution anemometers (flow sensors) for microfluidic applications with sensitivities and accuracies in the nL/min range have been on the market for a few years.[18−20] They have, for example, been used for the inline calibration of liquid chromatography systems.[21−23] In these sensors, the liquid flows through a small channel in a microchip or capillary, where at its center, a heating element adds a minimal amount of heat to the liquid (Figure 2).

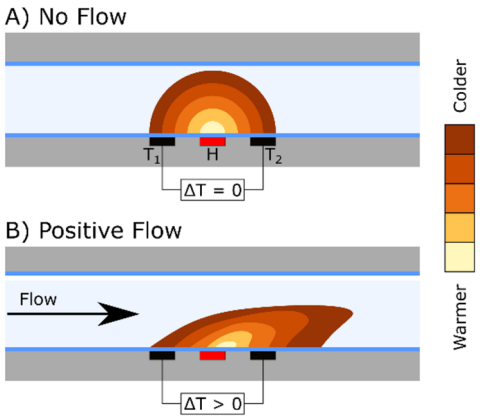

Figure 2. Inside the flow sensor: The liquid passes through an internal channel in the flow sensor (bright blue). An integrated heater (H) in close proximity to the fused silica wall locally heats up the liquid inside the channel, while the temperature difference (ΔT) between two temperature sensors (T1 and T2) is measured. (A) If there is no flow, the temperature profile is uniform, hence T1 = T2, and ΔT = T2 − T1 = 0. (B) If there is flow in the positive direction, the temperature profile gets distorted and T1 < T2, and ΔT = T2 − T1 > 0.

Two temperature sensors, one upstream and one downstream of the heater, measure the temperature of the liquid. The temperature difference between the two sensors is zero when there is no flow and gets larger the faster the liquid is moving through the channel. One commercially available version is, e.g., the LG16 series from Sensirion AG (Stäfa, Switzerland). It can

measure flow rates up to 7 μL/min with an accuracy of 5% of the measured value (m.v.) or 0.3% of the full scale (f.s.), whichever error is larger. The repeatability is 0.5% m.v. or 0.05% f.s. In general, this sensor can easily be connected to a CE capillary by commercial compression fittings, and pressure-driven flow through the capillary can accurately be measured through an electrical interface. Additionally, the sensor's wetted material is solely fused silica, the same material as the capillary itself, which helps to maintain the EOF. Nevertheless, the direct contact of the fluid flowing through this sensor type prevents the application of high voltage (HV), as the voltage could break through the sensor and the electrical connection, compromising the equipment and CE analysis.

To overcome this problem, an LG16−0150 flow sensor in combination with an in-house, custom-designed high voltage interface was used. The CE capillary (Series 106815 from Molex Polymicro, 50 μm inner diameter (i.d.), 363 μm outer diameter (o.d.)) was connected to the flow sensor with standard compression fittings (C-NNFFPK from Valco Instruments Co. Inc., USA), in combination with a PEEK tubing sleeve (1/32″ o.d. × .015″ i.d., part no. 1568, cut to length from IDEX HS, USA). Because the capillaries exhibit an internal diameter of 50 μm, the −0150D over the −0025D sensor version was chosen for this study, for which the sensor's internal diameter (i.d.) of the fluid channel is 150 μm versus 25 μm. If the flow sensor's i.d. were smaller than the capillary's, it would act as a choke point. Since the transition from the capillary to the larger i.d. of the sensor would disrupt the sample plug, it was installed after the detector. The maximum flow rate for the −0150D is 8 μL/min and 1.7 μL/min for the −0025D version. On the basis of the nature of this sensor to measure minute temperature differences within the flowing medium, it allows us to precisely assess the absolute temperature of the liquid. This temperature measurement (S1 of the Supporting Information) can provide important information, such as current or flow estimates based on Joule heating, the potential of BGE to form bubbles due to elevated temperatures, and temperature-induced peak broadening.

The sensor is mounted to a custom printed circuit board (PCB) along with its power and communication lines (Figure 3A−D). The PCB is powered by a 9 V battery and houses a microcontroller (ARM Cortex-M0+ STM32L0, STMicroelectronics, Switzerland) that handles the direct communication with the flow sensor via I^2C protocol. This board is connected to a second PCB via high voltage tolerant optocouplers (OPI1268S, TT Electronics, United Kingdom), which use light as a means of communication instead of electrical signals to isolate the sending and receiving end electrically. The second PCB is then connected to a computer or the CE instrument itself. The two optocouplers allow for bidirectional communication via the microcontroller to the flow sensor while electrically isolating the sensor's communication terminal, even when high voltage is applied. UART was chosen as the serial protocol to communicate via the optocouplers since it allows for two unidirectional lines, one for transmitting (Tx) and one for receiving (Rx) data, ideal for the unidirectional optocouplers. Additionally, in contrast to other protocols such as SPI and I^2C, no clock or chip select signal is required, therefore also reducing the number of required optocouplers.

The flow sensor floats at the applied potential while it is powered by the battery, which is also referenced to this floating potential. The microprocessor firmware, as well as the hardware, is designed to minimize power consumption to extend battery life. Instead of using optocouplers for high-voltage-compatible

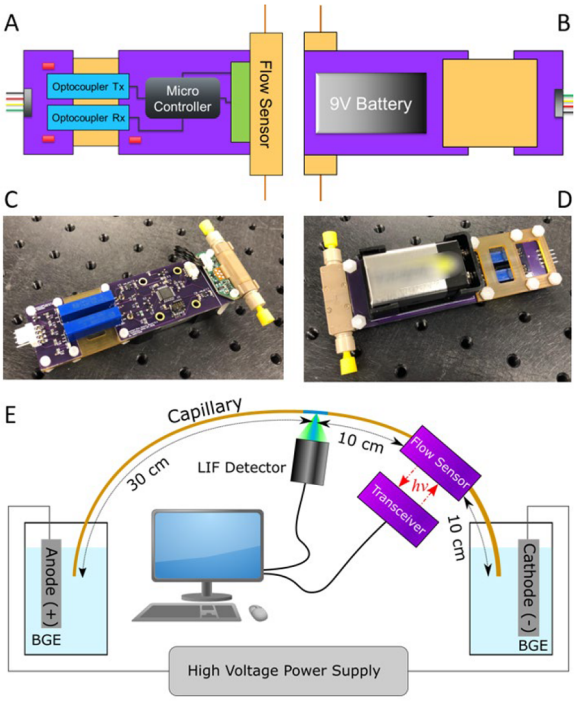

Figure 3. Schematic representation of the high voltage flow sensor for CE, top (A) and bottom view (B). The capillary (brown) is connected to the flow sensor. A microcontroller communicates with the flow sensor as well as the isolated "outside world" via two high voltage optocouplers (blue). The isolated portion is powered by a 9 V battery. The communication terminal is connected to the isolated PCB via cables (black, red, yellow, and green) and exchanges data via standard serial communication protocols. Photographs of the HV flow sensor interface: Top view (C) and bottom view (D). (E) Schematic representation of where the flow sensor is located in the custom CE-LIF instrument.

means of communication, one could also use wireless transmission such as WIFI, Bluetooth, or similar. The reason for this high voltage isolation is to protect both the operator and the measurement equipment. Besides the two optocouplers, the two PCBs are mechanically connected via a CNC machined bracket made from poly(ether imide) (PEI), an amorphous thermoplastic commonly used in high voltage electrical insulation applications.

This HV flow sensor was installed in a custom-built CE instrument equipped with a laser-induced fluorescence detector (CE-LIF). The system comprised a grounded BGE reservoir with platinum (Pt) anode, a 40 cm long capillary (30 cm to the LIF detection window) with an i.d. of 50 μm (same capillary as above), then the HV flow sensor, followed by a 10 cm long capillary with an i.d. of 100 μm (TSP100375, Polymicro Technologies, USA) terminated in a high voltage reservoir, also equipped with a Pt cathode (Figure 3E). The larger capillary, 100 μm i.d., same o.d. (363 μm), was used to reduce the voltage drop between the cathode and the detector and also to reduce the risk of bubbles getting stuck inside the flow sensor. A high voltage power supply (UM20N4/C/T/M from Spellman Corp., NY, USA) provided up to −20 kV to the cathode and was controlled and monitored using an in-house built controller board.[24] Controlled pneumatic pressure (0−15 psi) applied to the anode reservoir allowed for capillary conditioning and hydrodynamic injection of the sample plug. The custom epifluorescent LIF detector used a 488 nm laser (QFLD-488−

20S, QPhotonics, MI, USA) for the excitation of the fluorescent label and a photomultiplier tube (PMT) (H10721−210, Hamamatsu, Japan) for the emission signal detection.[25,26] The LIF signal, separation voltage, and the current were recorded at 8 Hz, and the flow and temperature inside the capillary at 2.5 Hz. In accordance with the datasheet, the response time to flow changes is 40 ms. The exact details of the CE-LIF instrument are beyond the scope of this report and will be described elsewhere. The goal is to demonstrate the working principle of this high-voltage-compatible flow sensor, which is independent of the CE system used. To underline the potential of the presented method, the custom CE system used closed reservoirs, and the height of the reservoirs relative to each other, as well as the overall system temperature, were not tightly controlled. These are all factors that can contribute to parasitic flow inside the capillary and are relevant for portable, *in situ*, and also potentially low-cost CE systems.

Chemicals and Reagents. Sodium tetraborate (STB), dimethylformamide (DMF), methanol, hydrochloric acid (HCl), sodium hydroxide (NaOH), fluorescein, and amino acids were purchased as analytical grade reagents from Sigma-Aldrich (St. Louis, MO, USA). 5-Carboxyfluorescein succinimidyl ester (CFSE) was obtained from Invitrogen of ThermoFisher Scientific (Waltham, MA, USA). All aqueous solutions were made with 18 MΩ × cm water.

A fluorescein standard was prepared at 10 mM in water and diluted in water to 10, 100, or 500 nM before analysis by CE-LIF. A standard solution of L-Ala, -His, -Ser, -Val, and Gly (hereafter referred to as "Mix5 solution") was prepared at 5 μM in 50 mM STB. A concentrated standard mixture was labeled (1 μM Mix5, 20 μM CFSE) and left to react at room temperature for 2 h then kept in the refrigerator. Samples were diluted in water to 100 nM daily before analysis by CE-LIF.

Experimental Setup. To demonstrate the working principle of the presented approach, a set of experiments were conducted: (a) a simple measurement of the flow rate versus applied voltage, (b) electromigration and detection of one single compound (fluorescein), and (c) separation and detection of a mix of five amino acids labeled with CFSE: (a) The flow rate versus applied voltage (S2 of the Supporting Information) was measured to prove the basic working principle of the high voltage flow sensor and its capability to acquire the volumetric flow inside the capillary despite the application of a high voltage potential. First, the capillary was conditioned for 5 min with 0.1 N NaOH, followed by water for 5 min, and then 50 mM STB for 5 min. With just the BGE inside the capillary (no sample injection), the voltage was ramped from 0 to −15 kV at −1 kV steps every 30 s, while recording the volumetric flow rate. (b) Hydrodynamic injections of sodium fluorescein dissolved in water at three different concentrations (10, 100, and 500 nM) were performed at 3 psi injection pressure for 500 ms. Three different concentrations were chosen to investigate whether there is a concentration dependency on the proposed method. The electrophoretic separation was executed at −15 kV, and triplicate measurements were performed per fluorescein concentration. The LIF signal, applied voltage, current, temperature and flow were recorded in parallel. (c) Labeled Mix5 solution was diluted in water to 100 nM and hydrodynamically injected at 3 psi for 500 ms. Three separations were performed at −10 kV, and three at −15 kV, while again simultaneously recording LIF signal, applied voltage, current, temperature, and flow.

RESULTS

The electropherograms for the nine fluorescein samples, three at 10, 100, and 500 nM each, are depicted in Figure 4A. The average migration time for all nine runs was 9.24 ± 0.33 min, with an average relative standard deviation (RSD) between the three triplicates of 3.54%. In this electropherogram, the LIF signal intensity is plotted versus the migration time t_p, as commonly done in capillary electrophoresis.

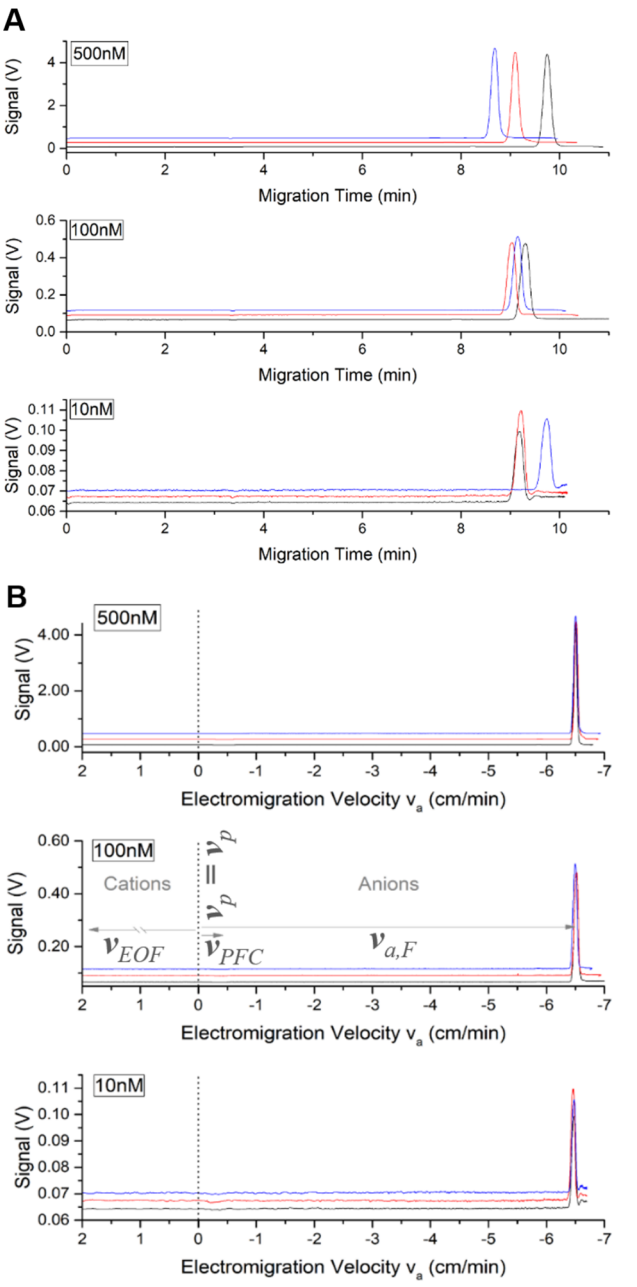

Figure 4. (A) Triplicate electropherograms at 10, 100, and 500 nM fluorescein in water expressed as signal versus migration time. BGE was 50 mM sodium tetraborate and separation voltage −15 kV. (B) Same measurements but corrected with flow sensor data and plotted versus analyte electromigration velocity v_a. Negatively charged anions exhibit a negative electromigration velocity, whereas it would be positive for cations under the same conditions. Signals are plotted slightly offset along the *y*-axis for better visibility.

Since the volumetric flow inside the capillary was recorded in parallel with the separation (see S3 of the Supporting Information), the migration time can be converted with eqs 1−6) to the electromigration velocity of the analyte v_a.

In contrast to Figure 4A, the x-axis in Figure 4B does not represent the migration time t_m, but the electromigration velocity v_a in cm/min. The scale of the x-axis was reversed to allow for easier visual comparison between the two graphs, with negative values to the right-hand side of the y-axis.

The average electromigration velocity for fluorescein v_{aF} was −6.49 ± 0.01 cm/min, with an average RSD between the three triplicates of 0.14%. This represents an improvement of more than 25× compared to the original data, whereas traditional compensation based on a neutral marker shows peak position RSD of 0.59%. Fluorescein is an anion and therefore migrates toward the anode or "against the EOF", which results in a negative v_{aF}. The signal rectification enabled by the flow sensor can also visually be confirmed by the almost perfectly overlapping peaks in Figure 4B compared to the peaks in Figure 4A. The peak height remains unchanged as the conversion from migration time to electromigration velocity does not affect the signal intensity. At $v_a = 0$, the migration velocity v_p and the volumetric flow velocity are equal (eq 6), and neutral species comigrate at $v_a = 0$, as they are not attracted to either pole. If there were any detectable cations in the sample, they would be expected to appear on the positive side of the x-scale. The flow sensor data for these measurements is discussed in more detail in the Supporting Information.

To demonstrate that this novel method also works for multiple analytes, triplicate separations of five CFSE-derivatized amino acids (100 nM Mix5 in water) were performed at −15 kV (Figure 5A). The average RSD for migration times was 3.32%. When converted to analyte electromigration velocity v_a, the average RSD dropped to 0.44%, or an improvement of the repeatability over all five amino acid peaks by a factor of 7.5.

The same experiment was repeated at −10 kV. When the detector signals for the two separation voltages are plotted versus m/C instead of electromigration velocity v_a, the peaks now align (Figure 5B). The peak intensity and resolution remain lower for the −10 kV separation compared to the −15 kV, as one would expect at lower field strengths, which causes longer migration times and hence more time for the sample plug to diffuse. Hence, this technique can be used to compensate for peak shifts in the electropherograms that are caused by the fluctuating current and voltage. Interestingly, calculations with voltage alone do not provide such an improvement of peak alignment as "charge separation" methodology does. Voltage drop calculation on the separation capillary are provided in S4 of the Supporting Information.

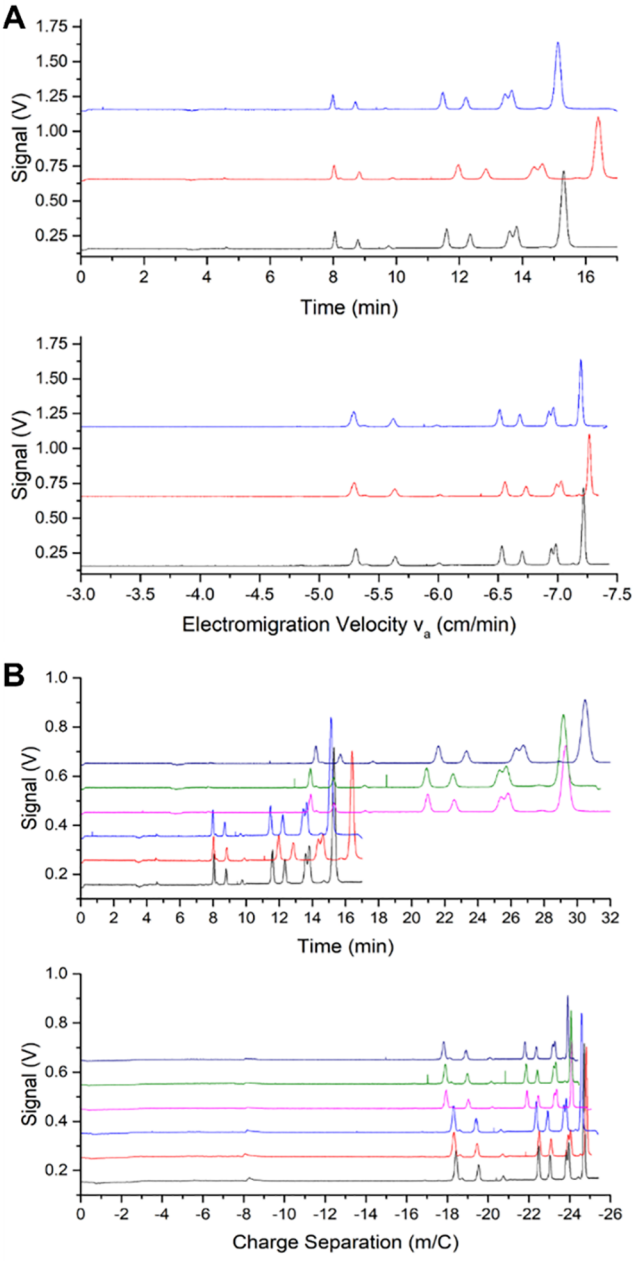

Figure 5. (A) Triplicate separations of Mix5, at a concentration of 100 nM in water. BGE was 50 mM sodium tetraborate and separation voltage −15 kV. Signals are plotted offset along the y-axis for better visibility. (B) Six separations or 100 nM Mix5, three at −15 kV (black, red, and blue), and three at −10 kV (pink, green, and purple). (Top) Standard electropherogram representation with signal versus migration time. (Bottom) Signal versus "charge separation".

CONCLUSION

In portable CE systems, gravity-driven flow can cause poor run-to-run reproducibility. The sensor described here can be a powerful tool to measure the EOF during CE separations in real time. This information can be used to correct the analytical data recorded by the detector, reducing ambiguities in peak identification. We demonstrated that measuring the volumetric flow inside the capillary during a separation allows for a powerful correction method of electropherograms, improved RSD, and it allows for better comparison between the acquired electropherograms. A previous study shows that plotting electrophoretic mobility instead of time for x-axis improves peak position repeatability almost up to five times.[27] However, said technique requires internal markers, whereas our proposed methodology is marker-free. Several attempts to plot electropherograms in another way than migration time on the x-axis are described in the literature. The inverted time domain, for example, allows for improving peak position repeatability.[28] Additional computational methods further improve qualitative and quantitative precision.[29] The transformation of raw electropherograms into continuous distributions allows visualizing the distribution of the chemical charge density or even molar mass.[30] These approaches can be used as a robust tool in metabolomics.[31]

Also, from an engineering perspective, this sensor can be helpful to monitor capillary conditioning (S5 of the Supporting Information), or also to optimize hydrodynamic sample injection. Moreover, the presented technology will help identify faults, such as a clogged capillary, and provide telemetry, which is critical for remotely controlled systems, e.g., for environmental monitoring or for spaceflight.

Theoretically, this approach might allow for the measurement of the hydrodynamic radius of the solutes (S6 of the Supporting Information).[32−35] The derived hydrodynamic radius of the fluorescein molecule in borate buffer was in the same order of magnitude as published in the literature.[36,37] One could envision plotting CE separations as signal versus hydrodynamic radius-to-charge ratio (r_H/z) instead of migration time, similar to mass spectrometry, where the spectra are expressed in m/z (mass over charge) ratios instead of time-of-flight. These "electropherospectra" for a given BGE could then be compared, independent of the system that acquired it.

The authors hope that this HV-compatible flow sensor will open new avenues for the CE community and aid in other fields where precision flow measurements at the high voltage side are necessary. It could potentially help improve dosing in electrospray-driven cancer treatment,[38] electrospray-based gene delivery,[39] electrospinning applications,[40] and electrospray-based propulsion systems.[41,42]

■ ASSOCIATED CONTENT

Supporting Information

The Supporting Information is available free of charge at https://pubs.acs.org/doi/10.1021/acs.analchem.2c00038.

Spreadsheet with raw data and step-by-step calculations on how to compensate the electropherograms with the flow sensor data is provided (XLSX)

Effect of temperature on flow rate (S1); applied voltage vs volumetric flow (S2); effect of flow rate on migration time (S3); voltage drop calculations (S4); effect of conditioning on electro-osmotic flow (S5); and estimation of hydrodynamic radius (S6) (PDF)

■ AUTHOR INFORMATION

Corresponding Author

Florian Kehl − *NASA Jet Propulsion Laboratory, California Institute of Technology, Pasadena, California 91109, United States;* Present Address: Innovation Cluster Space and Aviation (UZH Space Hub), Air Force Center, University of Zurich, 8600 Dübendorf, Switzerland; Present Address: Institute of Anatomy, Faculty of Medicine, University of Zurich, 8057 Zurich, Switzerland; Present Address: Institute of Medical Engineering, Space Biology Group, Lucerne University of Applied Sciences and Arts, 6052 Hergiswil, Switzerland; orcid.org/0000-0002-3242-8103; Email: florian.kehl@jpl.nasa.gov

Authors

Tomas Drevinskas − *NASA Jet Propulsion Laboratory, California Institute of Technology, Pasadena, California 91109, United States*

Jessica S. Creamer − *NASA Jet Propulsion Laboratory, California Institute of Technology, Pasadena, California 91109, United States;* orcid.org/0000-0003-2890-4901

Andrew J. DeMartino − *NASA Jet Propulsion Laboratory, California Institute of Technology, Pasadena, California 91109, United States*

Peter A. Willis − *NASA Jet Propulsion Laboratory, California Institute of Technology, Pasadena, California 91109, United States;* orcid.org/0000-0001-5394-1101

Complete contact information is available at: https://pubs.acs.org/10.1021/acs.analchem.2c00038

Notes

The authors declare no competing financial interest.

■ ACKNOWLEDGMENTS

The work in this article was done at the Jet Propulsion Laboratory, California Institute of Technology, under a contract with the National Aeronautics and Space Administration. Financial support was provided by JPL internal research programs and the NASA Postdoctoral Program (NPP) at the Jet Propulsion Laboratory, administered by Universities Space Research Association through a contract with NASA. U.S. Government sponsor is acknowledged.

■ REFERENCES

(1) Berg, C.; Valdez, D. C.; Bergeron, P.; Mora, M. F.; Garcia, C. D.; Ayon, A. *ELECTROPHORESIS* **2008**, *29*, 4914−4921.

(2) Drevinskas, T.; Maruška, A.; Girdauskas, V.; Dūda, G.; Gorbatsova, J.; Kaljurand, M. *Analytical Methods* **2020**, *12*, 4977−4986.

(3) Saar-Reismaa, P.; Erme, E.; Vaher, M.; Kulp, M.; Kaljurand, M.; Mazina-Šinkar, J. *Anal. Chem.* **2018**, *90*, 6253−6258.

(4) Mora, M. F.; Kehl, F.; Tavares Da Costa, E.; Bramall, N.; Willis, P. A. *Anal. Chem.* **2020**, *92*, 12959−12966.

(5) da Costa, E. T.; Neves, C. A.; Hotta, G. M.; Vidal, D. T. R.; Barros, M. F.; Ayon, A. A.; Garcia, C. D.; do Lago, C. L. *ELECTROPHORESIS* **2012**, *33*, 2650−2659.

(6) Kubáň, P.; Boček, P. *Anal. Chim. Acta* **2013**, *768*, 82−89.

(7) Ferreira Santos, M. S.; Noell, A. C.; Mora, M. F. *Analytical methods: advancing methods and applications* **2020**, *12*, 3205−3209.

(8) Ferreira Santos, M. S.; Cordeiro, T. G.; Noell, A. C.; Garcia, C. D.; Mora, M. F. *Electrophoresis* **2018**, *39*, 2890−2897.

(9) Willis, P. A.; Creamer, J. S.; Mora, M. F. *Anal. Bioanal. Chem.* **2015**, *407*, 6939−6963.

(10) Zamuruyev, K.; Ferreira Santos, M. S.; Mora, M. F.; Kurfman, E. A.; Noell, A. C.; Willis, P. A. *Anal. Chem.* **2021**, *93*, 9647−9655.

(11) Zhang, H.; Chen, H. *Analytical Methods* **2011**, *3*, 745−750.

(12) Seiman, A.; Vaher, M.; Kaljurand, M. *ELECTROPHORESIS* **2011**, *32*, 1006−1014.

(13) Drevinskas, T.; Maruška, A.; Naujokaitytė, G.; Telksnys, L.; Kaljurand, M.; Stanys, V.; Cowles, J.; Gorbatsova, J. *Chemija* **2020**, *31*, 146−155.

(14) Gaš, B. *High Performance Capillary Electrophoresis*; Agilent Technologies, Inc: Germany, 2018.

(15) Zhang, W.; He, M.; Yuan, T.; Xu, W. *ELECTROPHORESIS* **2017**, *38*, 3130−3135.

(16) Benhabib, M.; Chiesl, T. N.; Stockton, A. M.; Scherer, J. R.; Mathies, R. A. *Anal. Chem.* **2010**, *82*, 2372−2379.

(17) Xuan, X.; Li, D. *Journal of Chromatography A* **2005**, *1064*, 227−237.

(18) Tabata, O. *IEEE transactions on electron devices* **1986**, *33*, 361−365.

(19) Huijsing, J. H.; Schuddemat, J. P.; Verhoef, W. *IEEE Trans. Electron Devices* **1982**, *29*, 133−136.

(20) Mayer, F.; Paul, O.; Baltes, H. Flip-chip packaging for thermal CMOS anemometers. In *Proceedings IEEE The Tenth Annual International Workshop on Micro Electro Mechanical Systems. An Investigation of Micro Structures, Sensors, Actuators, Machines and Robots*; IEEE, 1997; pp 203−208.

(21) Li, D.; Chen, H.; Ren, S.; Zhang, Y.; Yang, Y.; Chang, H. *Sens. Actuators, B* **2020**, *305*, 127484.
(22) Termopoli, V.; Famiglini, G.; Vocale, P.; Morini, G. L.; Palma, P.; Rocío-Bautista, P.; Saeed, M.; Perry, S.; Cappiello, A. *Journal of Chromatography A* **2020**, *1627*, 461421.
(23) Ito, S.; Yoshioka, S.; Ogata, I.; Yamashita, E.; Nagai, S.; Okumoto, T.; Ishii, K.; Ito, M.; Kaji, H.; Takao, K.; Deguchi, K. *Journal of Chromatography A* **2005**, *1090*, 178−183.
(24) Kehl, F.; Cretu, V. F.; Willis, P. A. *HardwareX* **2021**, *10*, No. e00229.
(25) Cretu, V. F.; Kehl, F.; Metz, B. C.; Willis, P. A. *HardwareX* **2021**, *10*, No. e00233.
(26) Kehl, F.; Cretu, V. F.; Willis, P. A. *HardwareX* **2021**, *10*, No. e00240.
(27) González-Ruiz, V.; Gagnebin, Y.; Drouin, N.; Codesido, S.; Rudaz, S.; Schappler, J. *Electrophoresis* **2018**, *39*, 1222−1232.
(28) Mammen, M.; Colton, I. J.; Carbeck, J. D.; Bradley, R.; Whitesides, G. M. *Anal. Chem.* **1997**, *69*, 2165−2170.
(29) Schmitt-Kopplin, P.; Garmash, A. V.; Kudryavtsev, A. V.; Menzinger, F.; Perminova, I. V.; Hertkorn, N.; Freitag, D.; Petrosyan, V. S.; Kettrup, A. *Electrophoresis* **2001**, *22*, 77−87.
(30) Chamieh, J.; Martin, M.; Cottet, H. *Anal. Chem.* **2015**, *87*, 1050−1057.
(31) Codesido, S.; Drouin, N.; Ferré, S.; Schappler, J.; Rudaz, S.; González-Ruiz, V. *Electrophoresis* **2021**, *42*, 1875.
(32) Landers, J. P. *Handbook of Capillary and Microchip Electrophoresis and Associated Microtechniques*; CRC press, 2007.
(33) Weinberger, R. *Practical Capillary Electrophoresis*; Elsevier, 2000.
(34) Zhang, W.; Wu, H.; Zhang, R.; Fang, X.; Xu, W. *Chemical Science* **2019**, *10*, 7779−7787.
(35) Piaggio, M. V.; Peirotti, M. B.; Deiber, J. A. *ELECTROPHORESIS* **2005**, *26*, 3232−3246.
(36) Pu, Y.; Wang, W.; Dorshow, R.; Alfano, R. Picosecond polarization spectroscopy of fluorescein attached to different molecular volume polymer influenced by rotational motion. In *Organic Photonic Materials and Devices XIV*; International Society for Optics and Photonics, 2012, *825818*, 169−173.
(37) Mustafa, M. B.; Tipton, D. L.; Barkley, M. D.; Russo, P. S.; Blum, F. D. *Macromolecules* **1993**, *26*, 370−378.
(38) Ruzgys, P.; Böhringer, S.; Dokumaci, A. S.; Hari, Y.; Schürch, C. M.; Brühl, F.; Schürch, S.; Szidat, S.; Riether, C.; Šatkauskas, S.; Geiser, T.; Hradetzky, D.; Gazdhar, A. *Frontiers in Pharmacology* **2021**, *12*, 12.
(39) Boehringer, S.; Ruzgys, P.; Tamò, L.; Šatkauskas, S.; Geiser, T.; Gazdhar, A.; Hradetzky, D. *Sci. Rep.* **2018**, *8*, 4031.
(40) Luraghi, A.; Peri, F.; Moroni, L. *J. Controlled Release* **2021**, *334*, 463−484.
(41) Dale, E.; Jorns, B.; Gallimore, A. *Aerospace* **2020**, *7*, 120.
(42) Gassend, B.; Velasquez-Garcia, L. F.; Akinwande, A. I.; Martinez-Sanchez, M. *Journal of Microelectromechanical Systems* **2009**, *18*, 679−694.